strain
An International Journal for Experimental Mechanics

Fatigue Behaviour of SiC Particulate-Reinforced A359 Aluminium Matrix Composites

D. P. Myriounis*, T. E. Matikas† and S. T. Hasan*

*Materials & Engineering Research Institute, Sheffield Hallam University, City Campus, S11WB Sheffield, UK

†Department of Materials Science and Engineering, Materials Behaviour and Quality Control Laboratory, University of Ioannina, 45110 Ioannina, Greece

ABSTRACT: In this work, we describe the fatigue behaviour of silicon carbide (SiC_P)-reinforced A359 aluminium alloy matrix composite considering its microstructure and thermo-mechanical properties. A variety of heat treatments have been performed for the 20 vol. % SiC_p composite, which resulted in different strength and elongation behaviour of the material. The fatigue behaviour was monitored, and the corresponding S–N curves were experimentally derived for all heat treatments. The fatigue strength was found to depend strongly on the heat treatment. In addition, the fatigue behaviour was monitored non-destructively via the use of lock-in thermography. The heat wave, generated by the thermo-mechanical coupling and the intrinsic dissipated energy during mechanical loading of the sample, is detected by a thermal camera.

KEY WORDS: *fatigue, heat treatment, interface, metal matrix composites, thermography*

Introduction

The use of silicon carbide (SiC) particulate-reinforced aluminium alloy composites as a substitute of monolithic aluminium alloys in structural applications, especially in the aerospace and automobile industry, is becoming increasingly attractive. This is because of their superior strength, and stiffness, which is combined with their good performance in low cycle fatigue, corrosion fatigue and wear.

The mechanical behaviour of the aforementioned composites is dominated by the interface between the aluminium matrix and the SiC particles. While strengthening relies on the load transfer at the interface, toughness is influenced by the behaviour of the crack at the boundary between the matrix and the reinforcement, and ductility is affected by the relaxation of peak stresses near the interface because of the plastic flow ahead of the crack tip [1, 2]. As a result, the non-elastic behaviour of the composite is dominated firstly by the time-dependent stress field, i.e. the imposed stress rate, and secondly by the induced changes in the microstructure because of the presence of the reinforcement. These changes consist of segregation and precipitation caused by the thermal treatment that in turn is expected to drastically affect the fatigue strength and the fatigue life behaviour of the Al/SiC composites [3].

The response of the structural element to fatigue is critical for many applications. In the case of metal matrix composites (MMCs), the fatigue behaviour differs from that of unreinforced metals in several ways. In the case of particle-reinforced metals, numerous studies have focused on understanding the influence of the reinforcing particle on the matrix microstructure and the corresponding effect on the fatigue behaviour of the MMCs [4–8]. The size and percentage of the reinforcement are also affecting the fatigue life. In some cases, the fatigue strength may deteriorate by the addition of the reinforcement [9, 10]. The interaction of different mechanisms because of the presence of the reinforcement may lead to adverse effects on the fatigue life.

The fatigue strength of silicon carbide (SiC_P)-reinforced A359 aluminium alloy matrix composites has been reported to be mainly influenced by the thermo-mechanical processing history of the composite. Recent studies have discussed the influence of heat treatment on the interfacial strength and the mechanical properties of silicon carbide (SiC_P)-reinforced A359 aluminium alloy matrix composite [11]. The results indicated the interrelation between the heat treatment, the filler/matrix interface quality and the static failure mode of the composite. Further to the static properties, the heat treatment is expected to be of significant importance for the dynamic behaviour of these materials.

The scope of this study involved the application of two different heat treatment protocols on stripes of Al/SiC_P 20% specimens with the aim of tailoring the fatigue properties of the composite. As-received specimens have also been examined under fatigue. Fatigue tests were performed at three stress levels, and microstructural analysis of the fractured surface was performed using scanning electron microscopy (SEM). Simultaneously, the stress field on the sample was monitored non-destructively as imaged by the transient temperature gradient per fatigue cycle using lock-in thermography.

Material and Microstructure

The MMCs studied in this work consisted of aluminium–silicon–magnesium alloy matrix A359, reinforced with silicon carbide particles. Hot rolled A359 aluminium alloy with 20% SiC particles per weight with an average particle size of 17 ± 1 μm was used. In Table 1, the chemical composition of the matrix alloy is shown.

The Al–Si–Mg alloys are the most widely used in the foundry industry because of their good castability and high strength to weight ratio. Silicon improves the fluidity of aluminium in the molten state and, also, Si particulates improve the wear resistance of reinforced aluminium alloy. By adding magnesium, an Al–Si alloy becomes age hardenable through the precipitation of Mg_2Si particulates. An additional advantage of Al–Si alloys for casting applications is that silicon expands on solidification and Si is needed to

doi: 10.1111/j.1475-1305.2011.00827.x

Table 1: Chemical composition of the silicon carbide (SiC$_P$)-reinforced A359 aluminium alloy matrix composite

	Elements (wt %)					
Material	Si	Mg	Mn	Cu	Fe	Zn
A359/SiC$_P$ 20%	9.5	0.5	0.1	0.2	0.2	0.1

form Mg_2Si. The precipitation sequence is supersaturated solid solution $\rightarrow$ GP zones $\rightarrow$ β' $\rightarrow$ β (Mg_2Si) [12–14].

The microstructure of the composites was investigated in the as-received and heat-treated conditions, using a Philips XL40 Scanning Electron Microscope with a link 860 EDAX and a Philips FEI Nova Nano-Scanning Electron Microscope. The microstructure of the examined MMCs in the unetched, as-received condition (T1) has four distinct microphases as clearly marked on the image micrographs, which are as follows: the aluminium matrix, the SiC particles, the eutectic region of aluminium and silicon and the Mg phase (Figure 1A,B). SEM/mapping analysis has been also performed to confirm the above-mentioned phases. Al, Si and Mg elements were found present in the microstructure as shown in Figure 2.

The role of the reinforcement is crucial in the microdeformation behaviour. The addition of SiC to aluminium alloy increases strength and results in high internal stresses, in addition to the ones caused by the strengthening precipitates. Furthermore, the SiC-reinforced particles are not affected by the heat treatment process. A great deal of attention has been recently devoted for understanding the strengthening mechanisms in MMCs, which are distinguished by a large particulate volume fraction and relatively large diameter. Another important matter in understanding and modelling the strength of particulate MMCs is to consider the effect of particle shape, size and clustering [15, 16]. Lewandowski *et al.* [17] illustrated the important effects of clustering of reinforcement on the macroscopic behaviour as well as the effects of segregation to SiC/Al interfaces. Rozak *et al.* [18] presented the effects of casting condition and subsequent swaging on the microstructure, clustering and properties of Al/SiC composites.

The specimens under investigation have been manufactured by a stir-casting approach where the desired aluminium alloy is melted and carefully sized; ceramic (silicon carbide) particles are stirred in by means of an efficient vacuum-assisted mixing process [19]. The process allows good wetting and a very strong bond between the ceramic particles and aluminium matrix. The composites have then been hot cross-rolled. Even by this stir-casting approach, homogeneous distribution of the reinforcement cannot be achieved and therefore clustering and other forms of imperfections can occur. Some form of clustering has been observed (Figure 3) throughout the microstructural examination. This is mainly attributed to solidification shrinkage phenomena, but it is not considered as a major imperfection.

Heat treatment of composites though has an additional aspect to consider, the particles introduced into the matrix. These particles may alter the alloy's surface characteristics and increase the surface energies [20]. Within the scope of this study was to select the heat treatment cycle that produced the most favourable precipitate size and distribution pattern.

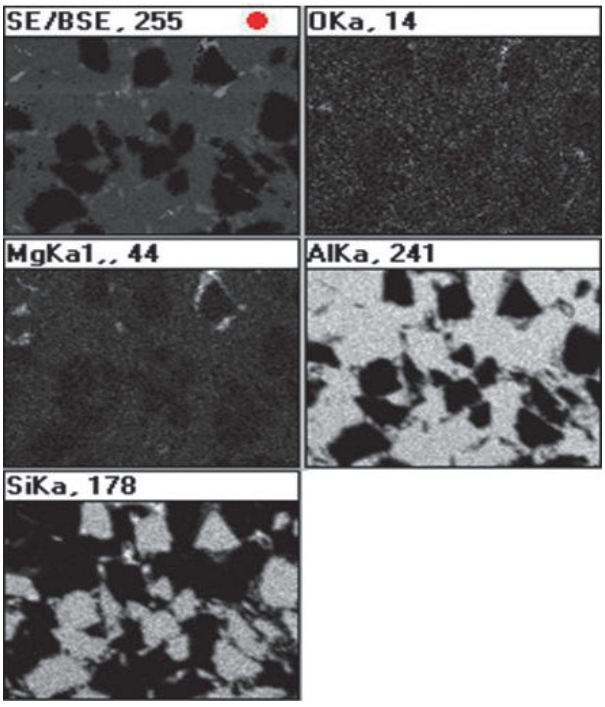

Figure 2: Scanning electron microscopy/Elemental Mapping analysis for Aluminium/SiC particulate Composite showing Al, Si and Mg elements present in the microstructure

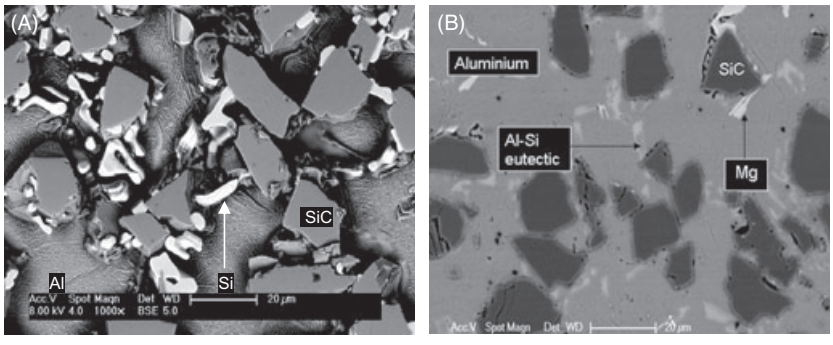

Figure 1: (A,B) Aluminium/SiC particulate composite showing Al, SiC$_p$, Al-Si eutectic, Si and Mg phases

doi: 10.1111/j.1475-1305.2011.00827.x

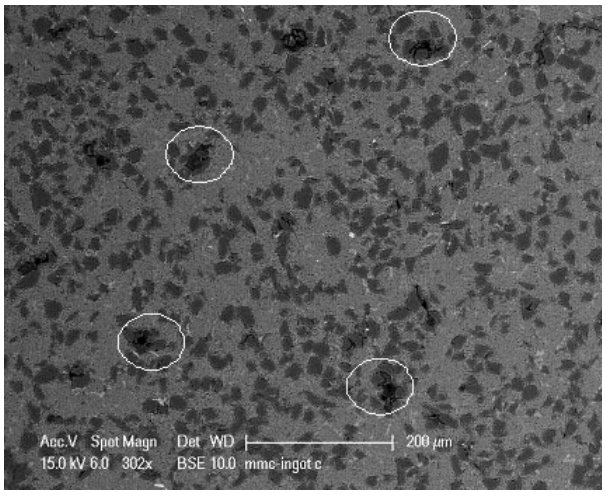

Figure 3: Clustering of SiC$_p$ observed in as received cross rolled microstructure

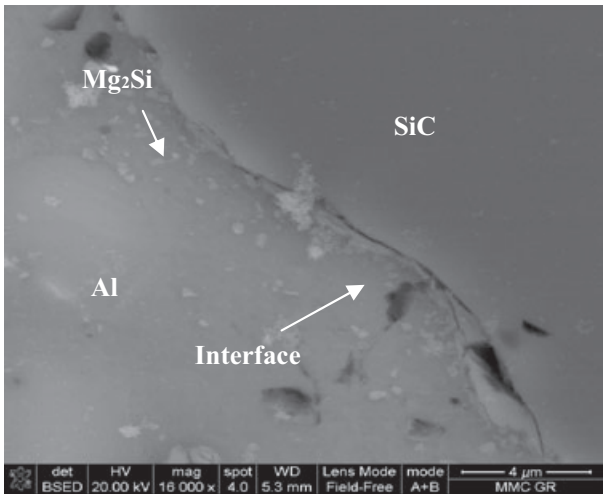

Figure 4: Hot rolled – T6 A359/20 vol. % SiC$_p$ showing interface of Al/SiC$_p$ and also small precipitates of Mg_2Si (white particles close to the interface)

Two different heat treatments were used for this study; T6 and modified T6 (HT-1) [21]. The two different heat treatments were selected to observe the different precipitation hardening mechanisms that can be produced. By controlling the solutionised temperature and time, the solute atoms are expected to dissolve at a different way and form the initial precipitate solid solution phases, while during the age hardening process those precipitates will grow.

The T6 heat treatment process consisted of the following steps: solution heat treatment, quench and age hardening. In the solution heat treatment, the alloys were heated to a temperature just below the initial melting point of the alloy for 2 h at 530±5 °C. Thus, all the solute atoms were allowed to dissolve to form a single-phase solid solution before being quenched in water. Next, the composites were heated to a temperature of 155 °C for 5 h and subsequently cooled in air. The microstructure of the heat-treated composite in this condition has been observed by using SEM microscopy and shows main phases indentified in the T6 condition as well as some Mg_2Si fully grown precipitates (Figure 4). Furthermore, the presence of Mg_2Si precipitates has been observed by XRD technique as shown in Figure 5.

The second heat treatment process was a modified T6 (HT-1) heat treatment, where the alloys in the solution treatment were heated to a temperature lower than the T6 heat treatment that is 450±5 °C for 1 h and then quenched in water. Subsequently, the alloys were heated to an intermediate temperature of 170 °C for 24 h in the age hardened stage and then cooled in air. This treatment is specific to alloy composition and the effect of addition of SiC and precipitation and segregation behaviour in terms of strength of MMCs. The microstructure in this condition does not show any fully grown precipitates formed (Figure 6) There are some β' rod shaped phases that are shown instead. This evidence shows that β' phase has been formed with magnesium and silicon reacting together but β phases forming platelets of precipitates have not been formed in this HT-1 heat treatment, and this is probably due to the solution treatment temperature that did not allow enough reactivity time for the kinetics dissolution of the main alloying elements [11].

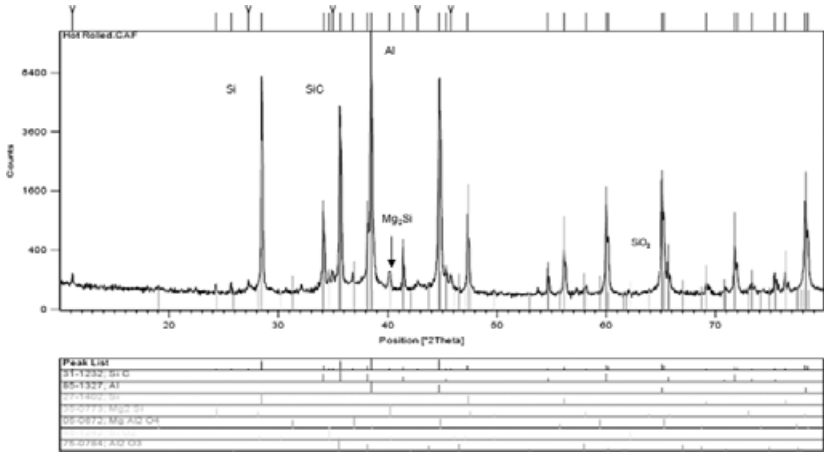

Figure 5: XRD of hot rolled – T6 A359/20 vol. % SiC$_p$ sample showing amongst phases the Mg_2Si phase

doi: 10.1111/j.1475-1305.2011.00827.x

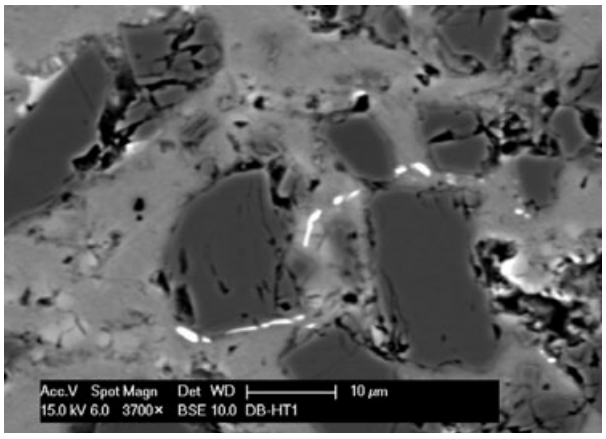

Figure 6: Hot rolled – HT1 A359/20 vol. % SiC_p showing rod shape β' phases of Mg_2Si around the matrix and the interface of the reinforcement

Experimental Work

Tensile properties

Prior to the fatigue testing, tensile tests were performed to determine the ultimate tensile strength (UTS) of the composites. Aluminium A359 with 20 vol. % SiC particulate composite specimens was tested in tension in the as-received state, and after two heat treatments: the previously described HT-1 and the standard T6 heat treatment. Tensile tests were conducted using a 100KN Instron hydraulic universal testing machine, and the strain was monitored using a clip gauge. The dimensions of the test coupons were 12.5 mm width, and 1.55 mm thickness. All the tensile tests were performed using 0.25 mm min^{-1} crosshead speed. At least three specimens were tested for each condition.

Fatigue testing

Tension-tension fatigue tests were conducted using a 100KN Instron hydraulic universal testing machine with complementary data acquisition computer and software. The system was operated under load control, applying a harmonic tensile stress with constant amplitude. By specifying the maximum and the minimum stress levels, the other stress parameters could be easily determined. These were the stress range, σ_r, stress amplitude, σ_a, mean stress, σ_m, and fatigue stress ratio, R ($=\sigma_{min}/\sigma_{max}$).

Throughout this study, all fatigue tests were carried out at a frequency of 5 Hz and at a stress ratio $R = 0.1$. Different stress levels between the UTS and the fatigue limit were selected, resulting in so-called Wöhler or S–N curves. Tests exceeding 10^6 cycles without specimen failure were terminated. Specimens that failed in or close to the grips were discarded. The geometry of the samples was the same as those used for the tensile characterisation, i.e. rectangular strips of 12.5 mm width, and 1.55 mm thickness.

Real-time thermographic characterisation

Thermography is a non-contact non-destructive technique that provides an image of the distribution of the temperature on the surface of the examined object. Using an adapted detector, thermography records the two-dimensional 'temperature' field as it results from the infrared radiation emitted by any object. The principal advantage of infrared thermography is its non-intrusive character. There has been substantial work carried out in this area, and plastic zone as well as crack growth has been monitored non-destructively in numerous papers [22–28].

The deformation of solid materials is almost always accompanied by heat release. When the material becomes deformed or is damaged and fractured, a part of energy necessary to initiate and propagate the damage is transformed in an irreversible way into heat [29, 30]. The heat wave, generated by the thermo-mechanical coupling and the intrinsic dissipated energy during mechanical loading of the sample, is detected by the thermal camera. The stress field has been monitored in relation to the cycles undergone by the sample. The important material property in radiation heat transfer is the emissivity ε of a test surface. The emissivity indicates the efficiency of a surface as a radiator of electromagnetic radiation. Blackbodies are the most efficient radiators and absorbers of electromagnetic radiation and have an emissivity of 1.0. All other bodies have an emissivity <1.0. To achieve an emissivity level as close as possible to that of a black body, a uniform coating of water soluble matt black paint was applied on the test samples. This allowed uniform heat transfer into (or from) the subject and produced a reasonably uniform emissivity [31]. All three fatigue stress levels were thermographically monitored for the 20% per weight Al/SiC composite. The thermographic image capture was set to 30 s per frame.

Results and Discussion

The results of the tensile tests for all the heat treatments of the MMCs are summarised in Table 2. The microhardness results of the samples for three different conditions, T6, HT1 and T1, are also tabulated. Details on the microhardness testing are reported in a previous publication [32].

In Figure 7, the fatigue behaviour of all studied systems is depicted. All systems exhibit typical S–N behaviour, reaching the fatigue limit before 10^6 cycles, which was set as the run-out point for the fatigue experiments. While the HT1 system failed at approximately the same absolute stress level as the T1 system, the S–N curve of the T6 system was shifted to considerably higher stress values. In this context, the T6 heat treatment yielded higher fatigue strength than both the T1 and HT1 systems. As can be observed, the heat treatment had significant influence on the fatigue response of Al/SiC_p composites. This is in agreement with previous observations [33], concluding that the heat treatment strongly affects both the static properties, as well as the failure mechanisms during quasi-

Table 2: Al/SiC_p 20% tensile testing and microhardness results

Material	Condition	$\sigma_{0.2}$ (MPa)	σ_{uts} (MPa)	ε (%)	E	$HV_{0.5}$
A359/ SiC_P-20%	T1	141	151	1.5	101	114
	HT-1	127	163	4.0	104	172
	T6	210	252	2.1	129	223

doi: 10.1111/j.1475-1305.2011.00827.x

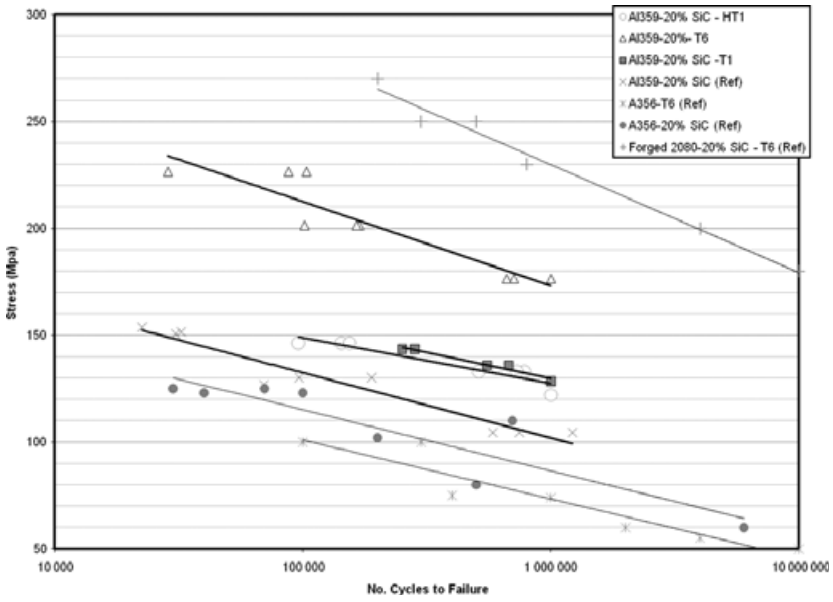

Figure 7: Stress amplitude versus fatigue cycles for various aluminum–SiC composite materials and aluminium alloys, including the present work

static tensile loading. It is also observed that aggressive heat treatment reduces the damage tolerance of the composites.

The results have been compared with some published fatigue data for similar composites as well as aluminium alloys [34, 35]. Specifically, and according to Figure 7 forged 2080 aluminium reinforced with 20% of SiC under T6 treatment exhibited higher fatigue strength compared with the composites used in this work. This may mainly attributed to the different nature of material forming and processing (forged, casted, cross-rolled, etc.), which plays an important role in the microstructural phenomena and consequently to the fatigue strength/behaviour of the composites. On the contrary, referenced A359-20% SiC and A356-20% SiC composites exhibited lower fatigue strength compared with this work's results.

It can be concluded that similar strengthening mechanisms present in those composites affect the fatigue strength and fatigue life performance. In addition, the fatigue slope for A356-T6 aluminium alloy shows high fatigue endurance limit but much lower fatigue strength values in comparison with the reinforced composites, showing that reinforcement plays a crucial role in the fatigue strength of the materials.

A direct comparison of the fatigue performance of the composite with the corresponding quasi-static performance in tension reveals some interesting details (see Table 1). Undoubtedly, the T6 heat treatment improved the strength of the composite. This can be attributed to a dominant mechanism related to the changes in the microstructure of the composite. This mechanism relates to the precipitates appearing in the microstructure of the composite at the vicinity of the interphase area, which results to the composite hardening. The creation of the interphase together with the improved stress transfer may be regarded as the main contributing parameters to the improved mechanical properties of the particulate-reinforced composite. The improved static strength is followed by a less spectacular performance in fatigue, with the fatigue limit of the material falling to the 70% of the UTS.

In this work, T6 specimens are quite brittle with low ductility compared with the HT1 specimens and therefore, crack initiation appears earlier at high stress levels, where the material's strain capability is not sufficient to impede crack initiation and propagation. This behaviour can be explained by the presence of high stress concentrations that in their turn are because of the embrittlement caused by the precipitates formed in the matrix and interfacial areas during the age hardening process. The lower HT1 heat treatment temperatures render the composite substantially more ductile than both the untreated (T1 specimens) and the T6 specimens.

When a crack approaches a reinforcing particle is either deflected by the hard reinforcement and continues around it or propagates through the reinforcement by cracking it. In the T6 condition, because of the strengthening of the matrix and interphase region with hard precipitates of Mg_2Si phases, the interface is much stronger. As the crack approaches the interphase area, the crack energy tends to be absorbed by the SiC particles, leading them to fracture and an overall rapid failure. Thus the reinforcement no longer plays the role of stress relief site but behaves in a brittle manner, with the crack propagating through it. In lower stress levels, the composite behaves in a different manner as the crack is arrested by the interphase.

Fractography has been employed to verify the aforementioned mechanisms. In the T6 condition, SiC particles seem to be cracked but not debonded (Figure 8A,B) indicating good interfacial bonding. It is usually the larger particles that break because of the higher probability of finding a flaw of critical size and because larger particles may have been cracked during fabrication. The extent of plastic zone ahead of the crack tip depends on the stress intensity factor. As a result, the number of particles within the elevated stress zone increases, resulting in a larger

doi: 10.1111/j.1475-1305.2011.00827.x

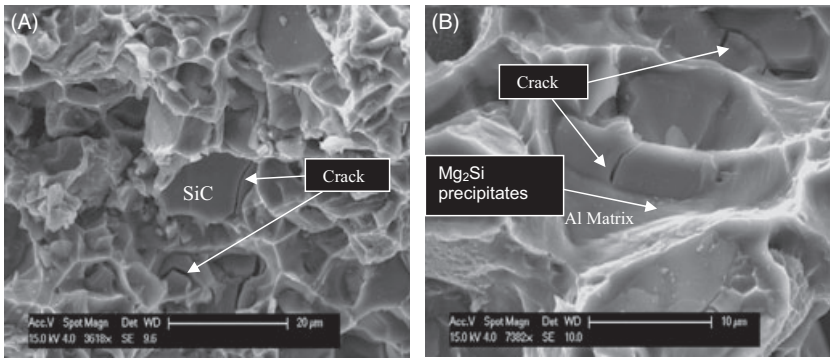

Figure 8: (A) T6 condition-SiC particles cracked but not debonded. (B) Cracked SiC particles-Mg_2Si precipitates formation

number volume of influence and finally to fracture. However, it is unclear that the breaking particles have much of an influence on the fatigue crack growth rate [36]. Furthermore, the small particles shown in Figure 8b are Mg_2Si precipitates produced during heat treatment. These precipitates seem to remain intact during fracture. Their small size eliminates their tendency to fracture.

As the fractographic examination revealed for the T6 condition, the fractured surface at 28 542 cycles at 90% of UTS fatigue (Figure 9A,B) showed striations formed in the aluminium matrix. This further supports the fact that high local stresses induce plastic flow of the matrix. As shown in Figure 9B, crack initiation occurred at the edge of the fractured surface. This crack defect at the edge of the sample is caused by extensive fatigue. In this fractured surface, ductile matrix and/or interfacial mechanisms cannot withstand and/or relieve the local stresses; therefore, the ceramic reinforcement (SiC_p) are exposed to extensive fatigue and higher stress concentrations, which eventually will lead to crack initiation.

HT1 specimen exhibited distinctly different behaviour. Fully grown precipitates were not observed, as it was in the case of T6 condition. However, the existence of other phases and especially β' phases appeared to improve the strength of the composite and most importantly its strain to failure. The HT1 composites exhibit slightly higher strength than the as-received composites but significantly enhanced ductility, and this is mainly attributed to the precipitation hardening mechanisms. These not fully grown precipitates act as relaxation mechanisms at the interfacial sites and at the same time strengthen the matrix (aluminium). Specifically for HT1 composites, the existence of these phases produced a much more homogenous microstructure, thus the strain to failure performance has been improved. The fractographic examination revealed that the interface bonding is not as good as in case of the T6 condition. HT1 condition exhibits lower static and fatigue strength than the T6 condition. In this case, the crack is propagated mainly through the interface region leaving the reinforcement intact (Figure 10A,B). The above postulation was validated by the clear evidence of debonded SiC reinforcement and the mark caused by the sliding of the reinforcement on the soft matrix (Figure 10B). Many similar marks have been indentified on the fracture surfaces examined. These marks may also be some form of striations. Owing to the presence of hard SiC particles, striation marks loose their appearance and appear on rough surface. Moreover Figure 10B shows evidence of striations on the ductile matrix as well as coalescence microvoids close by the SiC reinforcement.

The matrix ductility is also clearly indicated by the rippling effect caused by extensive fatigue of the sample (Figure 11A). As in the case of the T6 specimen, crack initiation sites were observed at the edge of the specimen surface (Figure 11B). Although the ductile nature of the HT1 treatment was obvious in the quasi-static tensile tests, its fatigue behaviour was not improved compared with the untreated T1 condition (Figure 7).

The T1 (as-received) condition composites were the least sensitive to fatigue testing. The T1 specimens exhibited a fatigue limit equal or higher to 85% of the UTS. As can be

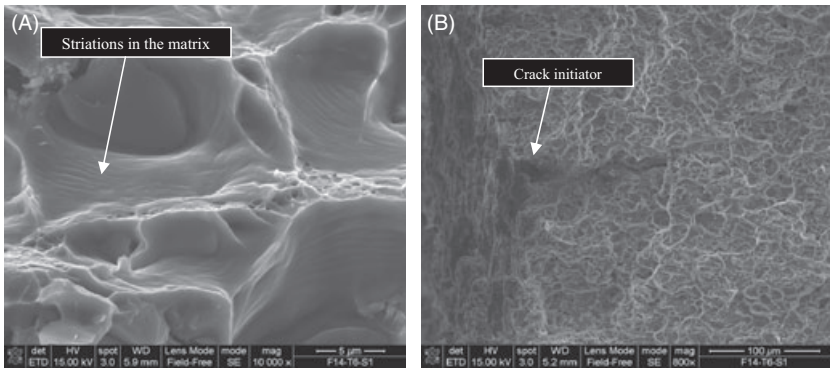

Figure 9: (A) T6 condition sample fractured surface at 226 MPa stress level fractures at 28 542 cycles-Striations shown in Al matrix. (B). Crack initiator at edge of fractured surface

doi: 10.1111/j.1475-1305.2011.00827.x

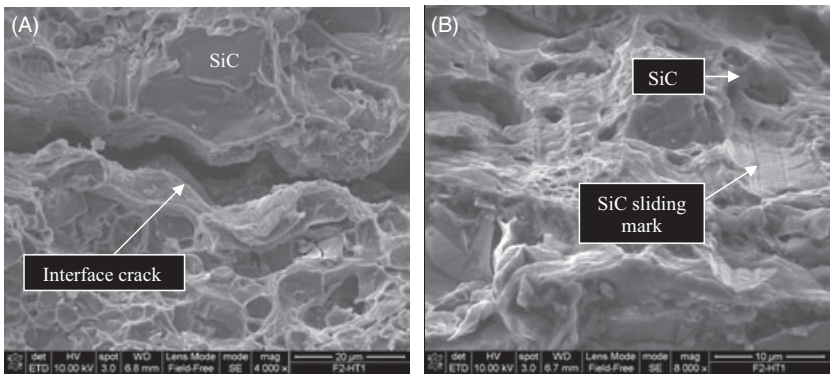

Figure 10: (A) Al/SiC$_p$ -HT1 condition- cracking through interface. (B) Sliding of SiC$_p$ on the Al matrix showing weak interface. Striations and coalescence microvoids also present

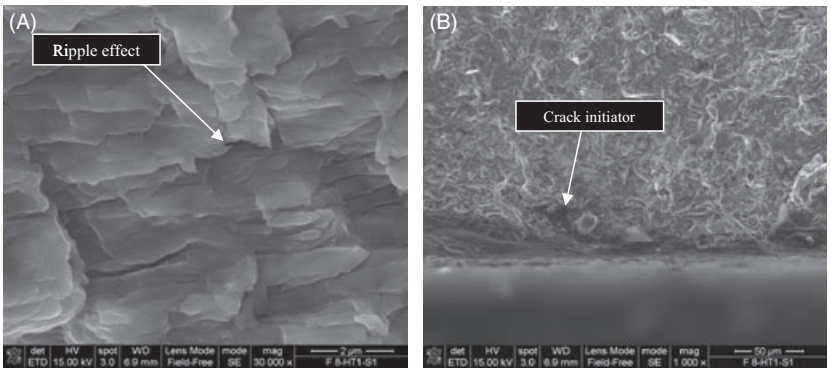

Figure 11: (A) HT1-Sample fractured surface at 133 MPa stress level fractures at 782 063 cycles-Rippling showing extensive fatigue. (B) Crack initiator close to surface edge

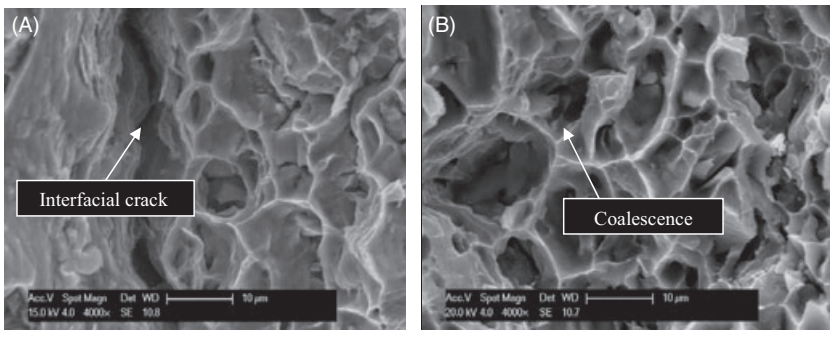

Figure 12: (A) T1 condition fatigue sample at 125 MPa stress level fractures around 1 000 000 cycles – Cracking through interface. (B) Coalescence microvoids evidence of ductile behaviour

seen in Figure 12A,B, the composite is clearly dominated by its ductile matrix, and the reinforcement plays a secondary role in the fatigue strength. The fractographic examination revealed the existence of coalescence that supports the aforementioned argument. Although the T1 specimens exhibited less ductile behaviour in quasi-static tension, this is not mirrored in the fatigue performance of the composites, where the untreated T1 condition performed equally well to the HT1 condition.

Finally, the thermographic characterisation revealed that the temperature/cycle slope rose more dramatically as the stress field increased. In Figure 13A,B,C, thermographic images are presented to demonstrate the development of damage close to the vicinity of the fracture area. As can be seen in Figure 13C just prior to fracture, the plasticity area is clearly delineated on the specimen's surface as a round

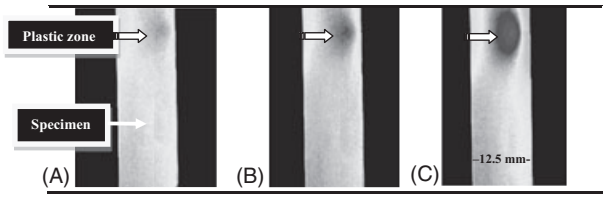

Figure 13: Thermographic images of fatigued Al/SiC composite specimen (T1 condition) at 143 MPa, showing the formation of plasticity zone before fracture occurs, (A) at *246 500* cycles, (B) at 248 600 cycles, and (C) at *251 861* cycles, which corresponds to the specimen's fracture point

doi: 10.1111/j.1475-1305.2011.00827.x

heated region that may be readily attributed to local plastic deformation. This real-time thermographic characterisation allowed the prediction of the fracture location of the specific sample approximately 25 min or 5361 cycles before failure occurs.

Conclusions

The tension-tension fatigue properties of Al/SiC$_p$ composites have been studied as a function of heat treatment. The possible damage development mechanisms have been discussed. The composites exhibited endurance limits ranging from 70 to 85% of their UTS.

The T6 composites performed significantly better in absolute values, but their fatigue limit fell to the 70% of their UTS. This behaviour is linked to the microstructure and the good matrix-particulate interfacial properties. The enhanced cohesion is mainly attributed to the strengthening mechanisms produced during heat treatment. These mechanisms in the case of T6 condition are the Mg_2Si fully grown precipitates that are reinforcing the matrix and produce a much better interfacial bonding.

In the case of the HT1 condition, the weak interfacial strength led to particle/matrix de-bonding, and this is because of the lack of fully grown precipitates. In the T1 condition, the fatigue behaviour is similar to the HT1 condition although the quasi-static tensile tests revealed a less ductile nature. In this condition, SiC reinforcement is the only strengthening mechanism present and does not affect to a great extent the fatigue behaviour of the composite. To conclude T6 condition showed the greater enhancement in the fatigue properties than the other two conditions. HT1 condition was expected to achieve higher values but the microstructure was pretty weak.

The above observations have been further supported by the metallographic examination of the fractured surfaces. Finally, thermographic images delineated the plasticity areas well before the failure of the specimen. This non-destructive evaluation tool is useful for analysing and studying fatigue and fracture mechanisms.

REFERENCES

1. Myriounis, D. P., Hasan, S. T., Barkoula, N. M., Paipetis, A. and Matikas, T. E. (2009) Effects of heat treatment on microstructure and the fracture toughness of SiC$_p$/Al alloy metal matrix composites. *J. Adv. Mater.* **41**, 18–27.
2. Manoharan, M. and Lewandowski, J. J. (1990) Fracture initiation and growth toughness of an aluminum metal-matrix composite. *Acta Met.* **38**, 489–496.
3. Hasan, S. T. (2005). Effect of heat treatment on interfacial strengthening mechanisms of second phase particulate reinforced aluminium alloy. In: *The 14th International Metallurgical and Materials\Conference (Metal 05)*, Czech Republic.
4. Taya, M. and Arsenault, R. J. (1989) *Metal Matrix Composites: Thermomechanical Behavior*, Vol. 4. Pergamon Press, Elmsford, New York.
5. Srivatsan, T. S. and Al-Hajri, M. (2002) The fatigue and final fracture behavior of SiC particle reinforced 7034 aluminum matrix composites. *Compos.: Part B – Eng.* **33**, 391–404.
6. Christman, T. and Suresh, S. (1988) Effects of SiC reinforcement and aging treatment on fatigue crack growth in an Al—SiC composite. *Mater. Sci. Eng.* **102**, 211–220.
7. Srivatsan, T. S. (1992) The low-cycle fatigue behaviour of an aluminium-alloy-ceramic-particle composite. *Int. J. Fatigue* **14**, 173–182.
8. Zhang, R. J., Wang, Z. and Simpson, C. (1991) Fatigue fractography of particulate-SiC-reinforced Al (A356) cast alloy. *Mater. Sci. Eng. A* **148**, 53–66.
9. Bloyce, A. and Summers, J. C. (1991) Static and dynamic properties of squeeze-cast A357-SIC particulate Duralcan metal matrix composite. *Mater. Sci. Eng. A* **135**, 231–236.
10. Hall, J. N., Jones, J. W. and Sachdev, A. K. (1994) Particle size, volume fraction and matrix strength effects on fatigue behavior and particle fracture in 2124 aluminum-SiCp composites. *Mater. Sci. Eng. A* **183**, 69–80.
11. Myriounis, D. P., Hasan, S. T. and Matikas, T. E. (2007) Role of interface on the mechanical behaviour of SiC-particle reinforced aluminium matrix composites. In: *Proceedings of the International Conference on structural analysis of advanced materials (ICSAM-07)*, Patras, Greece, September 2–6.
12. Strangwood, M., Hippsley, C. A. and Lewandowski, J. J. (1990) Segregation to SiCp/Al interfaces in al based metal matrix composites. *Scripta. Met.* **24**, 1483–1488.
13. Massalski, T. B. (1986) *Binary Alloy Phase Diagrams*. ASM International, Metals Park.
14. Vasudevan, A. K. and Doherty, R. D. (1989) *Aluminum alloys-Contemporary Research and Applications*. Academic Press, Inc, London Ltd., London.
15. Manoharan, M. and Lewandowski, J. J. (1989) In-situ deformation studies of an aluminum metal-matrix composite in a scanning electron microscope. *Scripta. Met.* **23**, 1801–1804.
16. Manoharan, M. and Lewandowski, J. J. (1992) Effect of reinforcement size and matrix microstructure on the fracture properties of an aluminum metal-matrix composite. *Mater. Sci. Eng. A* **150**, 179–186.
17. Lewandowski, J. J., Liu, C. and Hunt, W. H., Jr (1989) Effects of microstructure and particle clustering on fracture of an aluminum metal matrix composite. *Mater. Sci. Eng. A* **107**, 241–255.
18. Rozak, G., Lewandowski, J. J., Wallace, J. F. and Altmisoglu, A. (1992) Effects of casting conditions and deformation processing on A356 aluminum and A356-20% SiC composites. *J. Compos. Mater.* **26**, 2076–2106.
19. Skibo, M. D. and Schuster, D. M. (1988) US Patent 4,786,467.
20. Hasan, S. T., Beynon, J. H. and Faulkner, R. G. (2004) Role of segregation and precipitates on interfacial strengthening mechanisms in SiC$_p$ reinforced aluminium alloy when subjected to thermomechanical processing. *J. Mater. Process. Technol.* **153–154**, 757–763.
21. Merle, P. (2000) *MMC-assess Thematic Network, Thermal Treatments of Age Hardenable Metal Matrix Composites*, Vol. 2. MMC-assess Consortium), Vienna University of Technology, Vienna.
22. Stanley, P. and Chan, W. K. (1986) The determination of stress intensity factors and crack tip velocities from thermoelastic infra-red emissions. *Proc. Int. Conf. Fatig. Eng. Mater. Struct.*, IMechE, Paper **C262**, 105–114.
23. Tomlinson, R. A. and Olden, E. J. (1999) Thermoelasticity for the analysis of crack tip stress fields – a review. *Strain* **35**, 49–55.
24. Cavaliere, P., De Santis, A., Panella, F. and Squillace, A. (2009) Thermoelasticity and CCD analysis of crack propagation in AA6082 friction stir welded joints. *Int. J. Fatig.* **31**, 385–392.
25. Bremond, P. and Potet, P. (2001) Cedip infrared systems, lock-in thermography, a tool to analyze and locate

doi: 10.1111/j.1475-1305.2011.00827.x

thermo-mechanical mechanism in materials and structure Thermosence XXIII. *Proc. SPIE* **4360**, 560–566.
26. Choi, M.-Y., Park, J.-H., Kang, K. S. and Kim, W.-T. (2006) Application of thermography to analysis of thermal stress in the NDT for compact tensile specimen. *12th A-PCNDT 2006 – Asia-Pacific Conference on NDT, 5th–10th Nov*, Auckland, New Zealand.
27. Myriounis, D. P., Kordatos, E. Z., Hasan, S. T. and Matikas, T. E. (2011) Crack-tip stress field and fatigue crack growth monitoring using infrared lock-in thermography in A359/SiCp composites. *Strain* **47**, e619–e627.
28. Yang, B., Liaw, P. K., Peter, W. H. *et al.* (2004) Thermal-imaging technologies for detecting damage during high-cycle fatigue. *Metall. Mater. Trans. A* **35A**, 15–24.
29. Maldague, X. V. (2001) *Theory and Practice of Infrared Technology for Nondestructive Testing*. John Wiley & Sons, Inc,, New York.
30. ASM Handbook (1989) *Nondestructive Evaluation and Quality Control*, Vol. 17. ASM International.
31. Toubal, L., Karama, M. and Lorrain, B. (2006) Damage evolution and infrared thermography in woven composite laminates under fatigue loading. *Int. J. Fatigue* **28**, 1867–1872.
32. Myriounis, D. P., Hasan, S. T. and Matikas, T. E. (2007) Microdeformation behaviour of Al/SiC metal matrix composites. In: *The 6th International Symposium on Advanced Composites Proceedings (COMP07)*, Corfu, Greece.
33. Myriounis, D. P., Hasan, S. T. and Matikas, T. E. (2008) Heat treatment and interface effects on the mechanical behaviour of SiC-particle reinforced aluminium matrix composites. *J. ASTM Int. (JAI)* **5**, 7.
34. Rohatgi, P. K., Alaraj, S., Thakkar, R. B. and Daoud, A. (2007) Variation in fatigue properties of cast A359-SiC composites under total strain controlled conditions: effects of porosity and inclusions. *Compos. Part A: Appl. Sci. Manuf.* **38**, 1829–1841.
35. Wang, Q. G., Apelian, D. and Lados, D. A. (2001) Fatigue behavior of A356-T6 aluminum cast alloys. Part I. Effect of casting defects. *J. Light Metals* **1**, 73–84.
36. Davidson, D. L. (1993) Fatigue and fracture toughness of aluminium alloys reinforced with SiC and alumina particles. *Composites* **24**, 248–255.

doi: 10.1111/j.1475-1305.2011.00827.x